

Breast Tissue Characterization in X-Ray and Ultrasound Images using Fuzzy Local Directional Patterns and Support Vector Machines

Mohamed Abdel-Nasser¹, Domenec Puig¹, Antonio Moreno¹, Adel Saleh¹, Joan Marti², Luis Martin³ and Anna Magarolas³

¹Department of Computer Engineering and Mathematics, Rovira i Virgili University, Tarragona, Spain

²Dept. of Electronics, Computer Engineering and Automatics, University of Girona, Girona, Spain

³Hospital Universitari Joan XXIII de Tarragona, Tarragona, Spain

Keywords: Feature Extraction, Fuzzy Logic, Classification, X-ray Images, Ultrasound Images.

Abstract: Accurate breast mass detection in mammographies is a difficult task, especially with dense tissues. Although ultrasound images can detect breast masses even in dense breasts, they are always corrupted by noise. In this paper, we propose fuzzy local directional patterns for breast mass detection in X-ray as well as ultrasound images. Fuzzy logic is applied on the edge responses of the given pixels to produce a meaningful descriptor. The proposed descriptor can properly discriminate between mass and normal tissues under different conditions such as noise and compression variation. In order to assess the effectiveness of the proposed descriptor, a support vector machine classifier is used to perform mass/normal classification in a set of regions of interest. The proposed method has been validated using the well-known mini-MIAS breast cancer database (X-ray images) as well as an ultrasound breast cancer database. Moreover, quantitative results are shown in terms of area under the curve of the receiver operating curve analysis.

1 INTRODUCTION

Breast cancer is considered as one of the most dangerous cancers that attacks women (DeSantis et al., 2014). Early detection of breast cancer yields a reduction in mortality. *Mammographies* are the most effective method of breast cancer screening. In a mammography, each breast is compressed using compression plates, then it is X-rayed from top to bottom or by angle. In turn, *Sonographies* are safer and painless, and they generate real time images of the inside of the breast using ultrasound waves. *Breast density* is one of the main failure factors of mammographies because dense tissues may hide some tumour regions.

Breast density represents the relative amounts of fibroglandular and fat tissue in a woman breast (Lokate et al., 2010). The well-known mini-MIAS breast cancer database (Suckling et al., 1994) classifies the breast density into three categories: fatty, fatty-glandular and dense glandular (see Fig. 1). *Dense* breasts have more glandular and fibrous tissues, and they appear white in the mammogram. Therefore, they hide cancer regions, which also usually appear white in mammograms. In turn, *fatty* breasts have more fatty tissues and they can be seen grey in mammograms. Thus, it is easy to detect cancer in fatty breasts. Indeed, sonographies are superior

to mammographies in their ability to detect abnormalities in the dense breasts. Sonographies have become an important assistant to mammographies in breast cancer detection. They cannot replace a mammogram for breast screening, but they can provide more help to physicians.

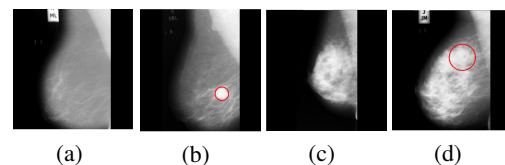


Figure 1: Mammogram examples in the mini-MIAS breast cancer database. *Fatty* mammogram containing: (a) normal and, (b) mass tissue (see the red circle). *Dense* mammogram containing: (c) normal and, (d) mass tissue (mass detection is not evident in this case).

Numerous computer aided diagnosis (CAD) systems have been proposed for breast mass detection with X-ray or ultrasound images. A breast mass CAD system usually consists of two main steps: *feature extraction* and *classification*. A comparison of various texture analysis methods for breast mass detection in X-ray images is presented in (Abdel-Nasser et al., 2014). For instance, Oliver et al. used the histogram of the local binary pattern (LBP) to reduce

the number of false positives of breast mass detection (Oliver et al., 2007). They used a support vector machine (SVM) for classification. Unfortunately, LBP may assign the same pattern to a pixel in a tumorous region and another pixel in a normal dense tissue, yielding a noticeable percentage of false detections. The histogram of oriented gradient (HoG) has also been used for breast mass detection (Pomponiu et al., 2014). HoG is used to train a SVM classifier. The cell size and the number of cells per block need to be optimized. If an unsuitable block size is used, the same HoG descriptor may be produced for a normal block and a tumorous block in dense mammograms leading to high number of false detections.

In turn, a discussion of the approaches used in ultrasound breast images CAD stages and a summary of their advantages and disadvantages are presented in (Shi et al., 2010). A breast cancer CAD system based on a fuzzy support vector machine is developed in (Shi et al., 2010) to automatically detect masses in ultrasound images. Moreover, *fuzzy local binary patterns (FLBP)* are proposed in (Keramidas et al., 2011). FLBP incorporate fuzzy logic in the representation of the local patterns in ultrasound images. FLBP are extracted from a set of regions of interest (ROIs) acquired from thyroid ultrasound images, and then a SVM classifier is used to classify them into nodule or non-nodule classes.

Noise, breast density and the variation in breast compressions yield a fuzzy appearance of the breast tissues. Unfortunately, the literature shows no consensus on an optimal feature set for mass/normal breast tissue classification, which means that the methods proposed in the literature don't produce a complete characterization of different tissues in breast images, yielding a high number of false positives (ROIs interpreted by a CAD system as abnormal when they are actually normal).

In this paper, the proposed work focuses on the *feature extraction* sub-task of breast cancer CAD system by proposing the *fuzzy local directional pattern (FLDP)* for characterizing breast tissues. The rationale behind the use of fuzzy logic is to compensate the uncertainty of the visual appearance of breast tissues due to noise, breast density and the variation in breast compressions. FLDP describes the shapes, margins, spots, edges, corners, junctions and other structures of different tissues in a breast region. FLDP is evaluated with mass/normal classification of ROIs extracted from X-ray, and ultrasound images.

The rest of this paper is organized as follows. Section 2 explains the related descriptors as well as the proposed descriptor. Section 3 explains the use of the proposed descriptor in breast tissue classification.

Section 4 includes the experimental results and discussion. Section 5 summarises our work, and suggests some lines of future work.

2 FUZZY LOCAL DIRECTIONAL PATTERN

This section comments the most related descriptors and explains in detail the proposed descriptor.

2.1 Related Descriptors

In (Oliver et al., 2007), LBP is used as a texture descriptor for reducing the number of false positives in breast cancer detection. The original LBP operator compares the intensity values of the eight neighbors of a 3×3 neighborhood around a pixel with the intensity value of this pixel. The corresponding bit of a neighbor pixel that has a higher intensity than the central pixel is set to 1 otherwise it is set to 0. Thus, each pixel is represented by 8 bits as shown in (Ojala et al., 2002). Thus, LBP depends on the intensity difference of the pixels that is very sensitive to noise and to illumination changes.

The *robust local binary pattern (RLBP)* is proposed in (Chen et al., 2013) to correct the non-uniform patterns in the LBP binary codes to reduce the effect of noise. Chen's method partitioned each 8-bit LBP binary code in sets of three consecutive bits. If *010* or *101* are found in the generated codes, they are replaced by *000* or *111* respectively. Chen's method converts a natural non-uniform pattern into a uniform pattern, which leads to a distortion in the overall description, because any wrong correction affects the final histogram.

Fig. 2 presents an example of the calculation of LBP codes for two different pixels, *A* and *B*: pixel *A* lays in a *tumorous* region, while pixel *B* belongs to a *normal* region. Although the two pixels are in completely different regions, LBP assigns the same binary code *00000000* to both of them, causing a dilemma in the classification stage (RLBP calculates the same codes).

The local directional pattern (LDP) is a robust grey scale texture descriptor that encodes the edge responses in a local neighbourhood. In this way, LDP reduces the reliance on the intensity difference used in LBP to be more robust against noise and changes in illumination. LDP computes the edge responses in eight directions by using compass Kirsch masks (Gonzalez and Woods, 2002). Jabid et al. proposed to set the top *k* responses positions to '1' and the other directions to '0' generating a 8-bit code for

each pixel (Jabid et al., 2010). Fig. 2 shows an example of the calculation of LDP codes. LDP assigns 00101001 to pixel A and 10100001 to pixel B. Although LDP generates different codes, the reliance on only the top three responses leads to a loss of information about a local neighbourhood.

In addition, the local directional number (LDN) is proposed in (Ramirez Rivera et al., 2013). In LDN, the edge responses are computed in eight directions by convolving the derivative-Gaussian masks with the original image. In (Ramirez Rivera et al., 2013), the derivative of a skewed Gaussian is used to create an asymmetric compass mask in order to get more robust edge responses against noise. The edge responses ($m_0, m_{45}, m_{90}, m_{135}, m_{180}, m_{225}, m_{270}, m_{315}$) were assigned to the location codes ($000, 001, 010, 011, 100, 101, 110, 111$), respectively. The LDN descriptor concatenates the location codes of the highest positive and the smallest negative responses to produce the final 6-bit descriptor of each pixel. Fig. 2 shows an example of the calculation of LDN codes. LDN can distinguish between pixel A and B by assigning different codes 100111 and 010111 , respectively. However, LDN may lose information about the neighbors in a certain neighbourhood because only the minimum and maximum responses are considered.

Finally, the *modified local directional pattern (MLDP)* is proposed in (Mohamed et al., 2014) to improve the robustness of optical flow estimation. MLDP encodes the edge responses computed by using the Kirsch compass masks based on a Gaussian filter. In Fig. 2, MLDP assigns 10000011 to pixel A and 10001011 to pixel B.

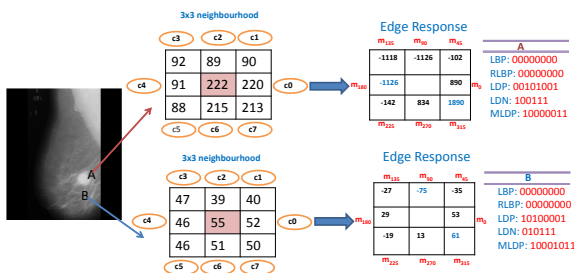


Figure 2: The binary codes generated with LBP, RLBP, LDP, LDN and MLDP for pixel A (tumorous) and pixel B (normal), $c_0 - c_7$ are the Kirsch compass masks presented in Fig. 4.

2.2 Proposed Descriptor

After identifying the main problems of the related descriptors, we propose FLDP as a texture descriptor for breast tissue characterization. FLDP describes a given pixel through its edge responses. The edge responses

ER of each pixel are computed using the Kirsch compass masks (see Fig.4). Given a certain pixel, its *eight* edge responses ER can be defined as such:

$$ER = \{ER_0, ER_1, \dots, ER_7\} \in \mathbb{R}^8 \quad (1)$$

Let A be the set of the ER greater than zero, and B the set of the ER smaller than zero:

$$A \equiv \{ER_i \mid 0 \leq i \leq 7, ER_i \geq 0\} \quad (2)$$

$$B \equiv ER - A \equiv \{ER_i \mid 0 \leq i \leq 7, ER_i < 0\} \quad (3)$$

In crisp approaches, a hard threshold is used to determine the prediction of each variable. In turn, fuzzy logic allows the use of a membership function to determine the class of each variable. In the fuzzification process, each input variable is mapped to its corresponding fuzzy variable according to a set of fuzzy rules (Zadeh, 1965). A and B can be defined as two fuzzy sets \tilde{A} and \tilde{B} , where \tilde{A} contains the *positive* edge responses, and \tilde{B} contains the *negative* edge responses. The fuzzy sets \tilde{A} and \tilde{B} can be expressed as such:

$$\tilde{A} \equiv \{(ER_i, \mu_+(ER_i)) \mid 0 \leq i \leq 7, \mu_+(ER_i) \geq \mu_-(ER_i)\} \quad (4)$$

$$\tilde{B} \equiv \{(ER_i, \mu_-(ER_i)) \mid 0 \leq i \leq 7, \mu_-(ER_i) > \mu_+(ER_i)\} \quad (5)$$

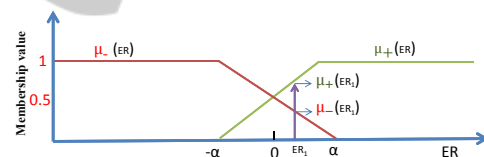


Figure 3: Linear membership functions, the green curve represents the membership function of the *positive* fuzzy set, whereas the blue curve represents the membership function of the *negative* fuzzy set.

Given an edge response, its degree of membership to these fuzzy sets can be computed. We used a linear function in order to calculate the degree of each edge response ER_i to be *negative*, or the degree of each ER_i to be *positive* (see Fig. 3). Let μ_+ define the degree of each ER_i to be *positive*:

$$\mu_+(ER_i) = \begin{cases} 0 & \text{if } ER_i < -\alpha \\ 0.5 + ER_i/2\alpha & \text{if } -\alpha \leq ER_i \leq \alpha \\ 1 & \text{if } ER_i > \alpha, \end{cases} \quad (6)$$

where α is a threshold. In addition, μ_- defines the degree of each ER to be *negative*:

$$\mu_-(ER_i) = 1 - \mu_+(ER_i) \quad (7)$$

Given the vector ER of a certain pixel, the degree of membership of each edge response to the *positive* and

negative fuzzy sets can be computed. Each edge response ER_i may belong to one of the following categories:

- a) $\mu_+(ER_i) = 1, \mu_-(ER_i) = 0, [ER_i \geq \alpha]$
- b) $\mu_+(ER_i) = 0, \mu_-(ER_i) = 1, [ER_i \leq -\alpha]$
- c) $\mu_+(ER_i) > 0, \mu_-(ER_i) > 0, [-\alpha < ER_i < \alpha]$

Let us define the subset of edge responses that belong to category c :

$$ER' = \{ER_i | 0 \leq i \leq 7, \mu_+(ER_i) > 0, \mu_-(ER_i) > 0\} \quad (8)$$

where $ER' \subseteq ER$. ER contains *eight* edge responses, and ER' is the subset of those edge responses in the fuzzy interval $[-\alpha, \alpha]$. For a given pixel, let us define the number of the elements in the subset ER' as $k = |ER'|, 0 \leq k \leq 8$. Given ER and ER' of a certain pixel, 2^k different 8-bits binary codes can be built as follows:

- If an edge response ER_i belongs to *category a*, ($\mu_+(ER_i) = 1, \mu_-(ER_i) = 0$), then all the 2^k codes will have '1' in position i of the binary code.
- If an edge response ER_i belongs to *category b*, ($\mu_+(ER_i) = 0, \mu_-(ER_i) = 1$), then all the 2^k codes will have '0' in position i of the binary code.
- The remaining k edge responses belong to *category c*, and the k bits associated to these k edge responses will be assigned different codes from $\underbrace{000\dots 0}_k \dots \underbrace{111\dots 1}_k$ in the 2^k binary codes to be built.

Fig. 4 presents an example of the calculation of FLDP with the threshold $\alpha = 100$. Both of $ER_2 = -10$ and $ER_3 = 30$ are located in the fuzzy interval $[-\alpha, \alpha]$. In this example, $k = 2$, so 2^2 FLDP codes are computed as follows:

- $ER_{0,1,6}$ belong to category b ('0' will be assigned to the associated positions).
- $ER_{4,5,7}$ belong to category a ('1' will be assigned to the associated positions).
- $ER_{2,3}$ belong to category c , consequently, *four* 2-bit combinations: '00', '10', '01' and '11', are assigned to the associated positions of $ER_{2,3}$ in the *four* 8-bits codes.

The critical parameter of FLDP is the selection of the proper value of the threshold α . The role of α in the generation of FLDP codes can be explained as follows:

- If α is big, most of the edge responses will belong to category c , and the number of the fuzzy cases (i.e. k) for each pixel will be high (in the limit, 256).

- If α is small, most of the edge responses will belong to categories a and b , and the number of fuzzy cases for each pixel will be low (in the limit, 1).
- If $\alpha = 0$, the calculations will be performed in the crisp space, i.e. there is no fuzzy interval. Consequently, the crisp sets of Eq.2 and Eq.3 will be used to calculate the binary codes. If the edge response is *positive*, '1' will be assigned in its associated position in the binary code. If the edge response is *negative*, '0' will be assigned in its associated position in the binary code.

In order to find the best value of α , a grid search procedure is used. In this paper, α is allowed to vary in the range of $10^2 \leq \alpha \leq 10^3$.

For each pixel, a set of m 8-bits binary codes ($1 \leq m \leq 256$) having values between 0 and 255 is generated. Each of these 8-bits codes $C = [c_0c_1\dots c_7]$ may be assigned a certain weight w_c , depending on the degree of the membership function of the associated edge response to the positive or negative fuzzy sets (depending on whether the bit in the code is '1' or '0', respectively). Given a binary code C , its weight w_c can be computed as follows:

$$w_c(C) = \prod_{i=0}^7 c_i \cdot \mu_+(ER_i) + (1 - c_i) \cdot \mu_-(ER_i) \quad (9)$$

Given a certain pixel with a set of edge responses from which 2^k codes have been generated, it can be proved that the addition of the weights of these 2^k codes is 1. Calling back the example of Fig. 4, we can use Eq. 6 and Eq. 7 to calculate the degree of membership of ER_2 and ER_3 to the positive and negative fuzzy sets as follows: $\mu_+(ER_2) = \mu_+(-10) = 0.45, \mu_-(ER_2) = 0.55, \mu_+(ER_3) = \mu_+(30) = 0.65, \mu_-(ER_3) = 0.35$. The weight of each fuzzy code can be calculated using Eq.9, $w_c(C_1) = 0.55 \times 0.35 = 0.1925, w_c(C_2) = 0.35 \times 0.45 = 0.1575, w_c(C_3) = 0.55 \times 0.65 = 0.3575, w_c(C_4) = 0.45 \times 0.65 = 0.2925$. It is clear that the addition of the weights (0.1925 + 0.1575 + 0.3575 + 0.2925) of the fuzzy codes of the pixel given in Fig. 4 equals 1.

The codes associated to a pixel may be represented graphically in a histogram in which the x-axis is the decimal value of each code (0-255) and the y-axis is the weight associated to that code. Given a grey level ROI, the complete FLDP histogram is computed by adding the weights of all the pixels in the input ROI (Ahonen and Pietikäinen, 2007).

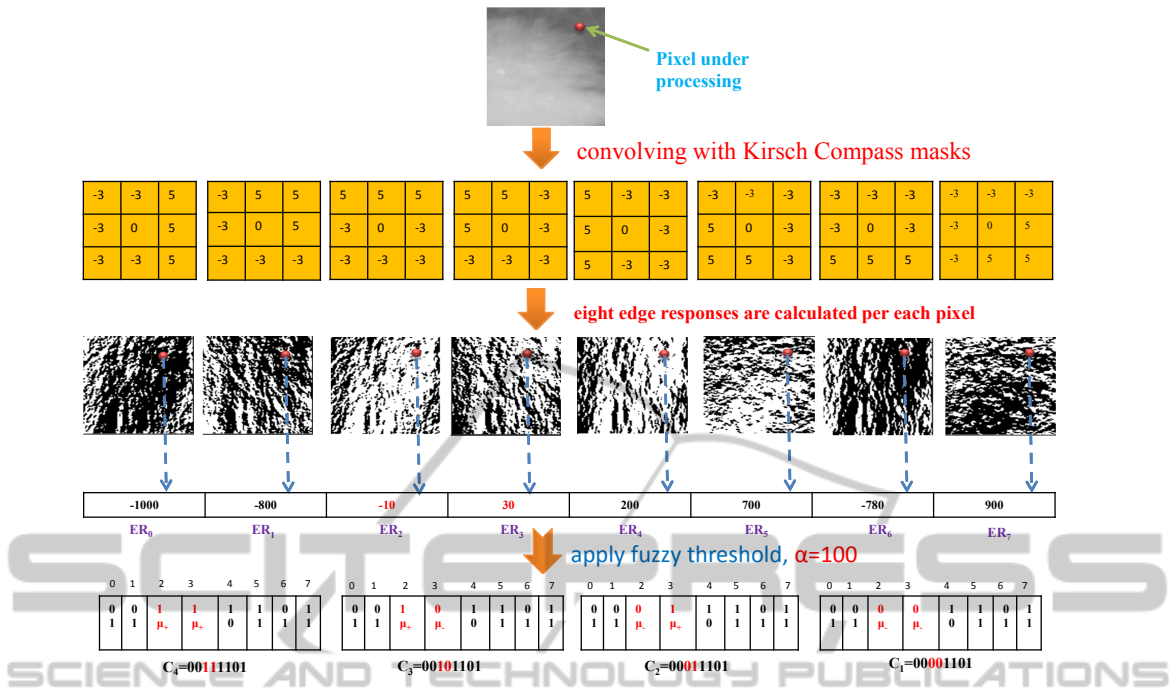


Figure 4: Example of the calculation of FLDP codes.

3 BREAST TISSUE CLASSIFICATION

In this paper, we put forward the claim that FLDP produces good characterization for different tissues in breast images. Given a set of normal and mass ROIs, FLDP is extracted from each ROI and fed to a SVM classifier. Then, the trained model is used to classify a query ROI as mass or normal.

3.1 Classification Stage

SVM is a supervised learning classifier that discriminates between positive and negative classes by finding a hyperplane that separates the classes. During the optimization process of SVM, the training data x_i are mapped to a higher dimensional space using a kernel function, $K(x_i, x_j) = (\phi^T(x_i) \cdot \phi(x_j))$. SVM uses the kernel trick, by which the data becomes linearly separable in the new space. The SVM classifier finds the hyperplane with a maximum separation between the classes in the new higher dimensional space. In the case of a *Linear SVM (LSVM)* classifier, ϕ refers to a dot product, whereas in a *Non-Linear SVM (NLSVM)* the classifier function is formed by non-linearly projecting the training data of the input space to a feature space of a higher dimension.

In this paper, we used a radial basis function

(RBF) as a mapping kernel, which is defined as follows:

$$K(x_i, x_j) = \exp\left(-\gamma \|x_i - x_j\|_2^2\right), \quad (10)$$

In this equation $\gamma = 1/2\sigma^2$, $\|x_i - x_j\|_2^2$ is the squared Euclidean distance between the two feature vectors x_i and x_j , and σ is a free parameter. In this paper, SVM classifier is implemented with Matlab, and based on libSVM library (Chang and Lin, 2011). In addition, a grid search algorithm was performed to find the optimum parameters of the RBF kernel (i.e., γ and the regularization parameter, C). In this work, we pre-set the ranges of the grid search algorithm with steps that equal 0.5 of the exponent. It searches for γ in the range of $2^{-5} < \gamma < 2^3$ and C is allowed to vary in the range of $2^{-5} < C < 2^{10}$.

3.2 Data Sets

The *mini-MIAS* breast cancer database (X-ray images) is used in our experiments (Suckling et al., 1994). It contains 332 images (1024×1024 pixels, pgm format) for 116 women in MLO view. The mini-MIAS database was created from the original MIAS database (digitised at 50μ pixel edge) by down-sampling it to 200μ pixel and clipping/padding it to a fixed size (this step was done by the authors of the database). The database has a ground truth (GT) provided by the radiologists and confirmed by a biopsy

test (*biopsy test* is an analysis of a sample from a suspicious breast tissue under a microscope). The GT of mini-MIAS shows the location of the abnormality, the radius of the circle enclosing the abnormal region, the characteristics of the background tissues and the breast density of each image.

In addition, a set of 267 breast B-mode ultrasound (US) images is used. The images were collected from 267 patients in UDIAT Diagnostic Centre of Sabadell (Spain) using a Siemens ACUSON Sequoia C512 system 17L5 HD linear array transducer (8.5 MHz). 104 of the images are normal and 163 images contain masses. The US database contains the GT of the lesions that appear in the abnormal image.

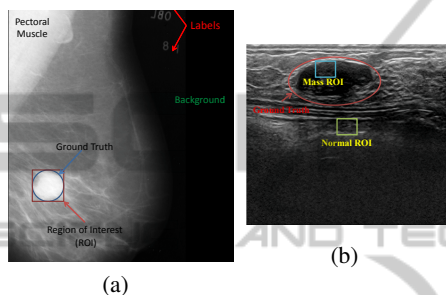


Figure 5: ROI generation using the GT of : (a) mini-MIAS, (b) US databases.

In order to generate the ROIs we followed the procedure given in (García-Manso et al., 2013). Fig. 5(a) presents an example of the GT of a mass region which is the *blue* circle, and the ROI that is the *red* square surrounding the circle. The ROIs of the normal tissues were randomly selected from the normal mammograms, and they were created with random sizes ranging from the smallest to the largest size found in the database. Fig. 5(b) presents an example of the normal and mass ROI generation in breast ultrasound images. With the mini-MIAS database, 109 mass ROIs were extracted from the mass mammograms and 203 normal ROIs were extracted from the normal mammograms. The extracted ROIs had different sizes, so they were resized into a fixed template (in this paper, 75×75 pixels). With the US database, 32×32 pixels ROIs were extracted (Keramidas et al., 2011). 107 mass ROIs and 300 normal ROIs were extracted from US images.

3.3 Evaluation

The performance of breast tissue classification using FLDP is measured in terms of the area under the curve (AUC) of the receiver operating curve (ROC) (Hanley and McNeil, 1982). We used the k -fold cross validation technique to generate the training and testing

data. In this procedure, the data are partitioned into k folds, $1/k$ of ROIs are used for testing and the rest of ROIs are used for training (in this work, $k=10$). We calculated the AUC value to evaluate the performance of FLDP with mass/normal breast tissue classification (AUC is averaged through the cross validation process).

4 EXPERIMENTAL RESULTS AND DISSCUSION

Fig. 6 (a) shows the receiver operating curve of the classification of the X-ray ROIs with LSVM and NLSVM classifiers. The best AUC value is achieved with the NLSVM classifiers. Fig. 6 (b) shows the ROC of classification of the US ROIs, in which the best result is also achieved with the NLSVM classifier.

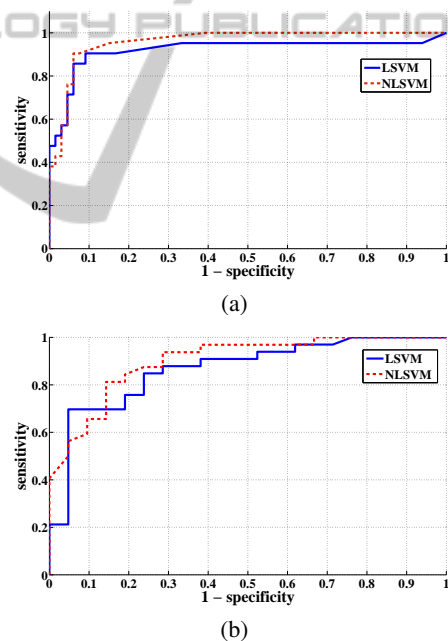


Figure 6: ROC curves of mass/normal breast tissue classification using FLDP with (a) X-ray and (b) US datasets.

As mentioned in Section 2, the critical parameter of the proposed descriptor is the threshold α . A *grid search* procedure is used to find the value of α which yields the best AUC value. In our experiments, the optimum value with the X-ray ROIs is 900, whereas with the US ROIs is 750.

In order to assess the performance of the proposed descriptor, a comparison between the best mass/normal classification results of the proposed

Table 1: Comparison between the AUC values of mass/normal breast tissue classification in the X-ray as well as US images using FLDP, FLBP, LBP, RLBP, HoG, LDP, MLDP, Gabor, and Haralick's features with LSVM and NLSVM classifiers.

Method	X-ray ROIs		US ROIs	
	LSVM	NLSVM	LSVM	NLSVM
FLDP	0.9203	0.9412	0.8665	0.9140
FLBP (Keramidas et al., 2011)	0.9010	0.9141	0.8915	0.8981
LBP (Oliver et al., 2007)	0.6978	0.8947	0.9012	0.8775
RLBP (Chen et al., 2013)	0.9103	0.9228	0.8398	0.8553
HoG (Pomponiu et al., 2014)	0.7664	0.8874	0.8810	0.8862
LDP (Jabid et al., 2010)	0.8195	0.7050	0.8350	0.9087
MLDP (Mohamed et al., 2014)	0.5404	0.5338	0.8408	0.8910
Gabor (Zheng, 2010)	0.6901	0.6412	0.7560	0.7388
Haralick's features (Soltanian et al., 2004)	0.6803	0.6217	0.8636	0.8882

descriptor and some of the state-of-the-art methods was performed. Table 1 presents the results of mass/normal breast tissue classification with the FLDP descriptor applied on the mini-MIAS database, as well as the results of mass/normal breast tissue classification with FLBP (Keramidas et al., 2011), LBP (Oliver et al., 2007), RLBP (Chen et al., 2013), HoG (Pomponiu et al., 2014), LDP (Jabid et al., 2010), MLDP (Mohamed et al., 2014), Gabor (Zheng, 2010) and Haralick's features (Soltanian et al., 2004). The aforementioned descriptors are calculated from the extracted ROIs, then they are classified with the same procedure used with FLDP (all descriptors are normalized to unit length).

Table 1 shows that MLDP, Gabor and Haralick's features produce the worst AUC values, indicating that they don't produce a robust description for the breast tissues in the X-ray images. Table 1 also shows that Gabor's features produce the worst AUC value with the US ROIs.

According to the experiments, FLDP produces the best results with the SVM classifiers. The other descriptors have many problems in the characterization of the breast tissues particularly in noisy images or with dense breasts. For instance, LBP and FLBP assign the same binary code for a pixel in a *tumorous* region and another pixel in a *normal dense* region. This happens when the values of all the neighbours are *higher/smaller* than the value of the centre pixel of a local neighbourhood.

In addition, Haralick's features depend on the co-occurrence matrix which calculates the number of the pixels having the same intensity at a certain offset (distance and angle). Unfortunately, a similar co-occurrence matrix is produced for a tumorous ROI and a normal ROI in a dense breast region. Moreover, the problem of HoG is the selection of the cell size and the number of cells per block. If an unsuitable block size is used, the same HoG descriptor will be produced for a dense normal block and a tumorous

block leading to a high number of false detections.

The key advantage of FLDP is the encoding of the edge responses of each pixel using fuzzy logic. Indeed, calculating the edge responses in eight different directions leads to a good characterization of the micro-patterns in a certain ROI. Consequently, if a micro-pattern is missed in a certain direction, it can be captured in other directions. In this way, FLDP describes the shapes, margins, spots, edges, corners, junctions and other structures of different tissues in a breast region. Unlike the methods used in the comparison, the use of the fuzzy logic provides a range of uncertainty, which gives FLDP the ability of generating binary codes that compensate the effect of deformations (because of compression), breast density variation as well as noise. In addition, the histogram that accumulates the weights of the FLDP codes increases the discrimination ability of FLDP, because it encodes both local information of each pixel as well as the global information of the a certain ROI.

5 CONCLUSION AND FUTURE WORK

In this paper, FLDP is proposed for breast tissue characterization. It properly discriminates between mass and normal tissues in both dense and fatty breasts. FLDP describes each pixel in a given image by its edge responses and makes use of fuzzy membership functions. We have used the well-known mini-MIAS breast cancer database as well as a breast US database in the experiments. In addition, LSVM and NLSVM classifiers are used to demonstrate the effectiveness of FLDP in discriminating between mass and normal tissues. The results show that the proposed descriptor leads to the best results when compared to some of the state-of-the-art descriptors (FLBP, LBP, RLBP, FLBP, HoG, LDP, MLDP, Gabor filter and Haralick's

features).

The immediate work is to extend the proposed descriptor FLDP to use higher order membership functions such as Gaussian and Trapezoidal functions. Future work will focus on the use of the neutrosophic logic instead of fuzzy logic. The neutrosophic logic is a general framework for unification of many existing logics including fuzzy logic. Thus, principles such as neutrosophic sets and neutrosophic probability will be used instead of fuzzy sets and the degree of membership.

ACKNOWLEDGEMENTS

This work was partly supported by the Spanish Government through project TIN2012-37171-C02-02.

REFERENCES

- Abdel-Nasser, M., Puig, D., and Moreno, A. (2014). Improvement of mass detection in breast X-ray images using texture analysis methods. In *Artificial Intelligence Research and Development: Proceedings of the 17th International Conference of the Catalan Association for Artificial Intelligence, Barcelona, Spain*, volume 269, pages 159–168. IOS Press.
- Ahonen, T. and Pietikäinen, M. (2007). Soft histograms for local binary patterns. In *Proceedings of the Finnish signal processing symposium, FINSIG*, volume 5, page 1.
- Chang, C.-C. and Lin, C.-J. (2011). Libsvm: a library for support vector machines. *ACM Transactions on Intelligent Systems and Technology (TIST)*, 2(3):27.
- Chen, J., Kellokumpu, V., Zhao, G., and Pietikäinen, M. (2013). Rlbp: Robust local binary pattern. In *Proc. of the British Machine Vision Conference (BMVC 2013)*, Bristol, UK.
- DeSantis, C., Ma, J., Bryan, L., and Jemal, A. (2014). Breast cancer statistics, 2013. *CA: A Cancer Journal for Clinicians*, 64(1):52–62.
- García-Manso, A., García-Orellana, C., González-Velasco, H., Gallardo-Caballero, R., and Macías-Macías, M. (2013). Study of the effect of breast tissue density on detection of masses in mammograms. *Computational and Mathematical Methods in Medicine*, 2013.
- Gonzalez, R. C. and Woods, R. E. (2002). *Digital image processing*. Prentice hall Upper Saddle River, New Jersey, USA.
- Hanley, J. A. and McNeil, B. J. (1982). The meaning and use of the area under a receiver operating characteristic (ROC) curve. *Radiology*, 143(1):29–36.
- Jabid, T., Kabir, M. H., and Chae, O. (2010). Facial expression recognition using local directional pattern (LDP). In *IEEE International Conference on Image Processing (ICIP)*, pages 1605–1608.
- Keramidas, E., Iakovidis, D., and Maroulis, D. (2011). Fuzzy binary patterns for uncertainty-aware texture representation. *Electronic Letters on Computer Vision and Image Analysis*, 10(1):63–78.
- Lokate, M., Kallenberg, M. G., Karssemeijer, N., Van den Bosch, M. A., Peeters, P. H., and Van Gils, C. H. (2010). Volumetric breast density from full-field digital mammograms and its association with breast cancer risk factors: a comparison with a threshold method. *Cancer Epidemiology Biomarkers & Prevention*, 19(12):3096–3105.
- Mohamed, M., Rashwan, H., Mertsching, B., Garcia, M., and Puig, D. (2014). Illumination-robust optical flow using local directional pattern. *IEEE Transactions on Circuits and Systems for Video Technology*, 24(9):1499–1508.
- Ojala, T., Pietikäinen, M., and Maenpää, T. (2002). Multiresolution gray-scale and rotation invariant texture classification with local binary patterns. *IEEE Transactions on Pattern Analysis and Machine Intelligence*, 24(7):971–987.
- Oliver, A., Lladó, X., Freixenet, J., and Martí, J. (2007). False positive reduction in mammographic mass detection using local binary patterns. In *Medical Image Computing and Computer-Assisted Intervention (MICCAI)*, pages 286–293. Springer.
- Pomponiu, V., Hariharan, H., Zheng, B., and Gur, D. (2014). Improving breast mass detection using histogram of oriented gradients. In *SPIE Medical Imaging*, pages 90351R–90351R. International Society for Optics and Photonics.
- Ramirez Rivera, A., Castillo, R., and Chae, O. (2013). Local directional number pattern for face analysis: Face and expression recognition. *IEEE Transactions on Image Processing*, 22(5):1740–1752.
- Shi, X., Cheng, H., Hu, L., Ju, W., and Tian, J. (2010). Detection and classification of masses in breast ultrasound images. *Digital Signal Processing*, 20(3):824–836.
- Soltanian, H., Rafiee-Rad, F., and Pourabdollah-Nejad D, S. (2004). Comparison of multiwavelet, wavelet, haralick, and shape features for microcalcification classification in mammograms. *Pattern Recognition*, 37(10):1973–1986.
- Suckling, J., Parker, J., Dance, D., Astley, S., Hutt, I., Boggis, C., Ricketts, I., Stamatakis, E., Cerneaz, N., Kok, S.-L., et al. (1994). The mammographic image analysis society digital mammogram database. In *2nd International Workshop on Digital Mammography*, pages 375–378. Excerta Medica.
- Zadeh, L. A. (1965). Fuzzy sets. *Information and control*, 8(3):338–353.
- Zheng, Y. (2010). Breast cancer detection with Gabor features from digital mammograms. *Algorithms*, 3(1):44–62.